Electronic Supplementary Material (ESI) for Journal of Materials Chemistry A.

Supporting information

Tailoring $LaMnO_3$ cathode for proton-conducting solid oxide fuel cells: Integration of high performance and excellent stability

Hailu Dai [a, 1], Xi Xu [b, c, 1], Chao Liu [a], Chengjian Ma [d], Qinfang Zhang [a] and Lei Bi [b, *]

a. School of Materials Science and Engineering, Yancheng Institute of Technology, Yancheng 224051, China

b. School of Resource Environment and Safety Engineering, University of South China, Hengyang 421001, China

c. Department of Materials, Imperial College London, Prince Consort Road, London SW72BP, UK

d. Analytical and Testing Center, Yancheng Institute of Technology, Yancheng 224051, China

[1] These authors contributed equally to this work

*Corresponding author

Email: lei.bi@usc.edu.cn, bilei81@gmail.com

Experimental section

Theoretical calculations were carried out by means of density functional theory using VASP (Vienna ab initio simulation package)[1-5]. All calculations were performed with a cutoff energy for the valence electrons of 500 eV, in a (4×4×4) gamma centered K-point mesh. The 2×2×2 supercell was used for the calculations. The oxygen vacancy formation energy could be calculated according to

$$E_f = E_{defect} + \frac{1}{2} E_{O_2} - E_{perfect},$$

where E_f is the oxygen vacancy formation energy, E_{defect} is the total energy of defective bulk, E_{O_2} is the energy of molecular oxygen and $E_{perfect}$ is the total energy of the stoichiometric bulk.

The hydration energy of the samples could be calculated according to

$$\Delta E_{hydration} = E_{2OH} - E_{defect} - E_{H_2O}$$

where $\Delta E_{hydration}$ is the hydration energy, E_{2OH} is the energy of the crystal with two additional protons, E_{defect} is the total energy of the defective bulk and E_{H_2O} is the energy of a single water molecule.

The energy barriers and transition states for proton migration were located by using the climbing image nudged elastic band (NEB) method[6]. The (001) surface was cleaved and the adsorption of O_2 and CO_2 was simulated to study the surface properties of the $La_{0.5}Ca_{0.5}MnO_{3-\delta}$ (LCaM) material. The O-O bond length for the O_2 molecular was calculated by putting an oxygen molecular in an empty box which kept the same size as the box for the surface relaxation and the oxygen adsorption relaxation, followed by the energy optimization of the oxygen molecular.

$La_{0.5}Ca_{0.5}MnO_{3-\delta}$ (LCaM) powder was synthesized by a wet chemical route, using La_2O_3, $CaCO_3$ and $(CH_3COO)_3Mn\cdot 2H_2O$ as the starting materials. Citric acid was used as the complexing agent. The preparation details can be found in our previous studies[7, 8]. The powder was calcined at 950 °C for 3 h to achieve pure phase. Anode-supported $BaZr_{0.1}Ce_{0.7}Y_{0.2}O_{3-\delta}$ (BCZY) half-cells were fabricated by the conventional co-pressing and co-sintering method and the co-sintering temperature was set at 1300 °C and the details can be found in our previous studies[9]. The LCaM cathode was deposited on the sintered BCZY electrolyte surface, followed by a co-firing procedure at 900 °C in the microwave sintering furnace. Then, the cell was tested with H_2 as the fuel and static air as the oxidant. The electrochemical performance of the cell was recorded using an electrochemical workstation (Squidstat Plus, Admiral Instruments). The morphology and the elemental distributions of the LCaM powder were observed by scanning transmission electron microscopy (STEM, JEM-2100F). The morphologies of the tested cell were observed using a scanning electron microscopy (SEM, Nova Nano SEM 450). The chemical stability of the LCaM powder was examined by exposing the powder in a CO_2-containing atmosphere (10% CO_2+90% air) at 600 °C, and the phase composition of the powder was detected with the in-situ high temperature X-ray diffraction (XRD) at 600 °C. The measurement was carried out every 30 minutes and the test was lasted for 12 h under the flowing CO_2. An additional treatment of the LCaM powder in the (10% CO_2+90% air) at 600 °C was carried out and the treatment was lasted for 100 h to further demonstrate the stability of LCaM against. The phase composition of the powder after the treatment was examined by XRD.

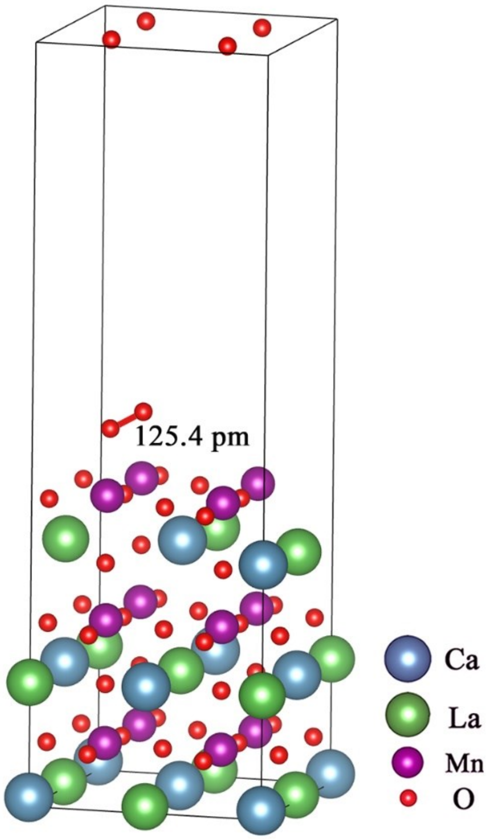

Figure S1. The calculated configuration for the adsorption of O_2 on the surface of LCaM.

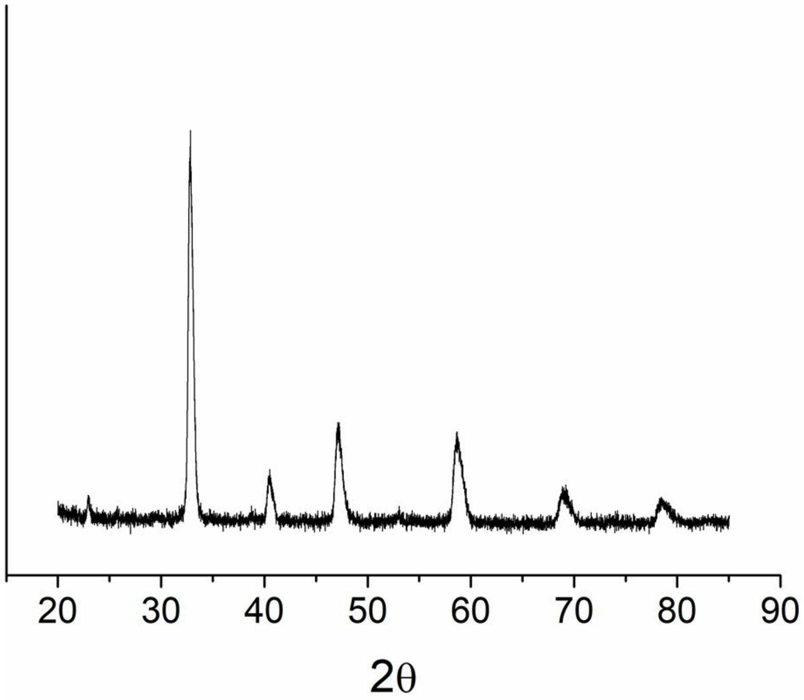

Figure S2. XRD pattern for the synthesized LCaM powder.

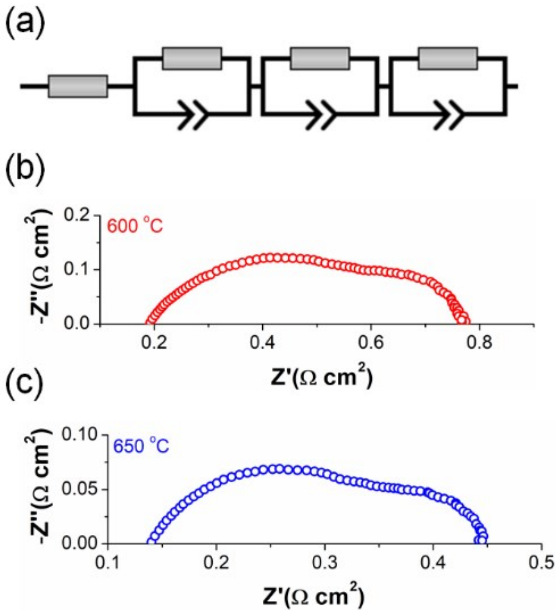

Figure S3. (a) The equivalent circuit used to fit the EIS plots; the EIS plots for the cell using the LCaM cathode tested at (b) 600 °C and (c) 650 °C.

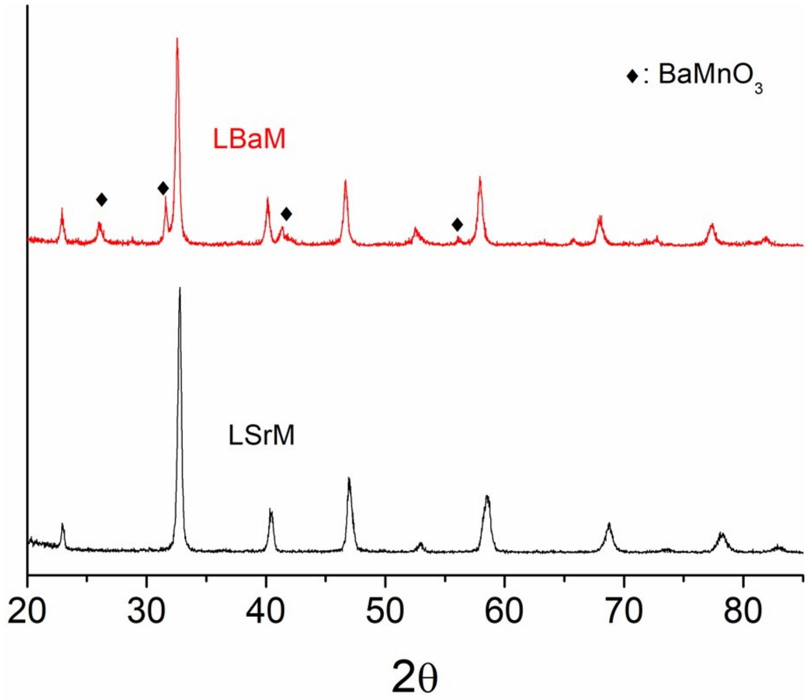

Figure S4. XRD patterns for the LSrM and LBaM powder after calcination.

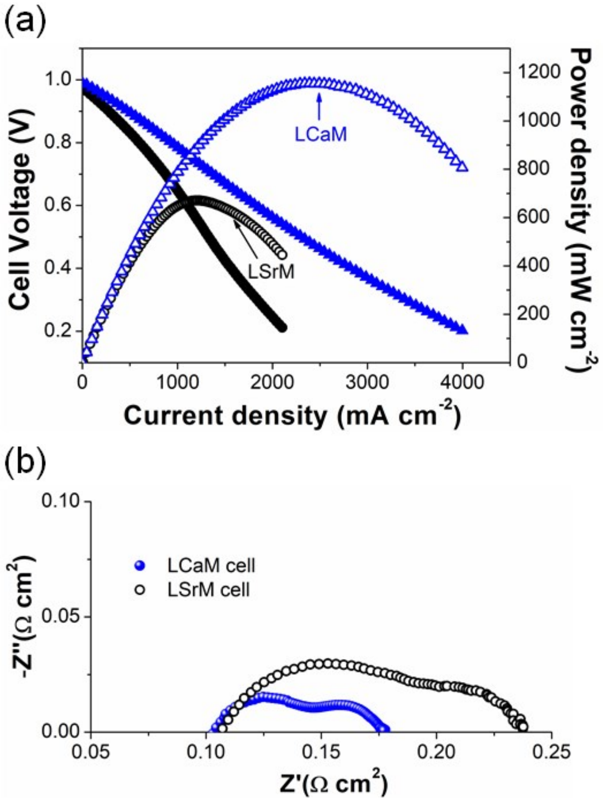

Figure S5. Comparison of (a) fuel cell output and (b) EIS plots for the LCaM cell and the LSrM cell, tested at 700 ^{o}C.

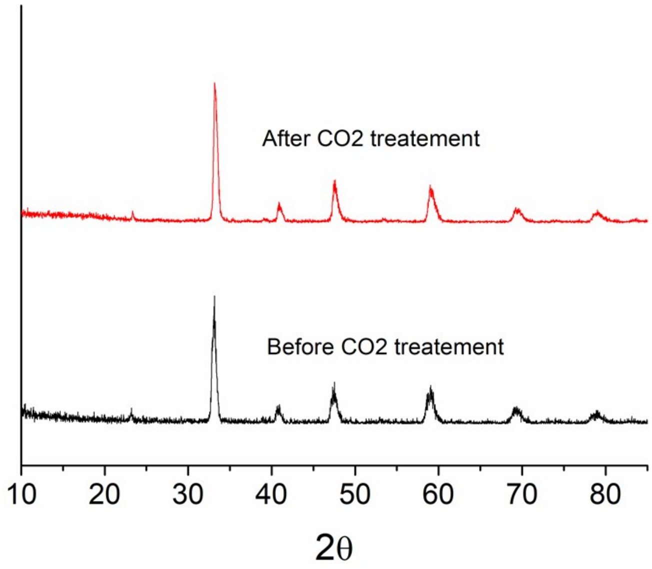

Figure S6. XRD patterns for the LCaM powder before and after the treatment in a CO_2-containing atmosphere at 600 ^{o}C for 100 h.

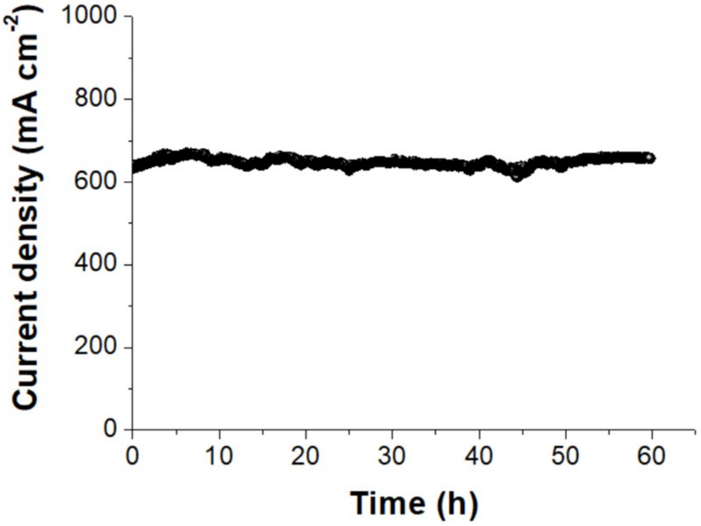

Figure S7. The stability test of the cell under an applied voltage of 0.6 V measured at 600 ^{o}C.

Table S1. The resistance contribution at high frequency (R_{HF}), middle frequency (R_{MF}) and low frequency (R_{LF}) for the LCaM cell tested at different temperatures, obtained from the EIS plot fitting.

Temperature (°C)	R_{HF} (Ω cm^2)	R_{MF} (Ω cm^2)	R_{LF} (Ω cm^2)
600	0.047	0.32	0.21
650	0.033	0.14	0.13
700	0.009	0.027	0.034

References

1. G. Kresse and D. Joubert, *Phys Rev B*, 1999, **59**, 1758-1775.

2. G. Kresse and J. Furthmuller, *Phys Rev B*, 1996, **54**, 11169-11186.

3. P. E. Blöchl, O. Jepsen and O. K. Andersen, *Phys Rev B*, 1994, **49**, 16223-16233.

4. W. Kohn and L. J. Sham, *Phys Rev*, 1965, **140**, A1133-A1138.

5. P. Hohenberg and W. Kohn, *Phys Rev*, 1964, **136**, B864-B871.

6. G. Henkelman, B. P. Uberuaga and H. Jónsson, *J Chem Phys*, 2000, **113**, 9901-9904.

7. X. Xu, L. Bi and X. S. Zhao, *J Membrane Sci*, 2018, **558**, 17-25.

8. L. Bi, S. P. Shafi, E. H. Da'as and E. Traversa, *Small*, 2018, **14**, 1801231.

9. B. Wang, X. H. Liu, L. Bi and X. S. Zhao, *J Power Sources*, 2019, **412**, 664-669.